Electrochimica Acta 338 (2020) 135788

Contents lists available at ScienceDirect

Electrochimica Acta

journal homepage: www.elsevier.com/locate/electacta

Electrochemical capacitors operating in aqueous electrolyte with volumetric characteristics improved by sustainable templating of electrode materials

Anetta Platek [a], Cristina Nita [b, c, d], Camélia Matei Ghimbeu [b, c, e, **], Elżbieta Frąckowiak [a], Krzysztof Fic [a, *]

[a] Poznan University of Technology, Institute of Chemistry and Technical Electrochemistry, Berdychowo 4, 60-965, Poznan, Poland
[b] Université de Haute-Alsace, Institut de Science des Matériaux de Mulhouse (IS2M), CNRS UMR 7361, F-68100, Mulhouse, France
[c] Université de Strasbourg, F-67081, Strasbourg, France
[d] Center for Advanced Laser Technologies (CETAL), National Institute for Lasers, Plasma and Radiation Physics, Atomistilor 409 bis, RO-77125, Magurele, Romania
[e] Réseau sur le Stockage Electrochimique de l'Energie (RS2E), CNRS FR3459, 33 Rue Saint Leu, 80039, Amiens Cedex, France

ARTICLE INFO

Article history:
Received 22 October 2019
Received in revised form
23 January 2020
Accepted 25 January 2020
Available online 31 January 2020

Keywords:
Carbon materials
Electrochemical capacitors
Sustainable energy storage
Aqueous electrolyte
Energy storage

ABSTRACT

Soft- and salt-templating methods have been combined to obtain highly microporous carbon materials with mesopores in the narrow pore size range. Phenolic resin was used as a carbon source, and rubidium and caesium chloride were used as salt-templates, giving a well-developed microporosity with a high specific surface area, whereas a sacrificial triblock polymer Pluronic F-127 (soft-template) induced the mesopores of essential importance for fast access of the electrode surface area for the electrolytic solution. The combination of a high specific surface area (up to 2556 $m^2\ g^{-1}$) with a suitable pore size (0.77 −0.88 nm) resulted in an excellent performance of the electrochemical capacitor. High specific energies of 16.7 $Wh \cdot kg^{-1}$ at 300 W kg^{-1} of specific power have been achieved for a CsCl-T-based high-voltage (1.5 V) device with a 0.5 $mol \cdot L^{-1}$ Li_2SO_4 electrolytic solution. The improved rate handling was allowed to maintain 10 $Wh \cdot kg^{-1}$ of specific energy at 4 kW kg^{-1} of specific power. In contrast to the other carbons with well-developed porosities, the material density obtained allowed our device to reach competitive, remarkably higher volumetric characteristics.

1. Introduction

The energy storage market, which is currently being stimulated by the increasing power demands of portable electronic devices and electric vehicles, has developed dynamically [1–6]. Many efforts have been made in order to design and implement novel materials for energy storage systems [7–10]. The miniaturization of electronic devices and fast-charging requirements have directed most of the research towards electrochemical capacitors (ECs) and Li-ion batteries [11]. The response time for ECs usually is in the domain of seconds because their principle of operation is based on the physical adsorption of ions in the so-called electric double-layer, which is formed at the electrode/electrolyte interface [12]. Such an energy storage mechanism ensures an excellent performance from the long-time perspective, due to the lack of structural changes in the electrode material. For this reason, ECs are used to store and release energy, for instance, during an incidental breakdown of power suppliers [13]. In batteries, the charge is stored by the redox processes (including intercalation and insertion processes), thus providing a very high energy density output with a moderate response time [11]. Hence, the application field for both systems is entirely governed by their *modus operandi*, and they are not intended to replace one another but to be complementary. However, since the kinetics of the chemical reaction is a kind of natural property of the matter and cannot be 'changed', the technological concerns suggest that the properties of the electrochemical capacitors are easier to tune. In fact, there is a continuing trend of increasing the energy density of electrochemical

* Corresponding author.
** Corresponding author. Université de Haute-Alsace, Institut de Science des Matériaux de Mulhouse (IS2M), CNRS UMR 7361, F-68100, Mulhouse, France.
E-mail addresses: camelia.ghimbeu@uha.fr (C.M. Ghimbeu), krzysztof.fic@put.poznan.pl (K. Fic).

https://doi.org/10.1016/j.electacta.2020.135788

capacitors, bringing them closer to battery systems, i.e., with specific energies on the level of tens and hundreds of $Wh \cdot kg^{-1}$. Unfortunately, this is quite a large challenge and in many cases (essentially when faradaic storage is incorporated to the charge accumulation mechanism, similar to in hybrid systems) the power is reduced remarkably. To some extent, such an effort does not make much sense, since high-power batteries have recently been put on the market and serve perfectly for short-term storage but have an otherwise very limited cyclability. Furthermore, such batteries are high-power only during their discharge but not during their charge, which is a needed characteristic for use in popular applications like regenerative braking energy storage. Therefore, a reasonable approach should be to optimize the energy and power density together with the long-term performance.

On the one hand, over the last 20 years, several concepts for tuneable carbon-based materials for ECs have been proposed. The short list of main discoveries needs to include activated carbons [14], carbon nanotubes (CNTs) [15–20], graphene [21], and carbon onions [9,22–24]. Such a variety of textural 'arrangements' implies different applications [7,19,25–34]. On the other hand, it is well-known that commercially available electrochemical capacitors are based on a cheap, abundant and chemically stable material, i.e., activated carbon.

The design of a new energy storage system requires many parameters to be considered: the conductivity of the components, the ion/pore size ratio, the micro to mesopores ratio and the recycling of the components after reaching end-of-life criterion [35–37]. Therefore, various precursors (mostly sourced from the biomass) [7] and synthesis methods (pyrolysis, activation, sol-gel, templating…) [38–40] have been proposed. To obtain micro/mesoporous carbons, various activation methods have been proposed, i.e., chemical or physical. The main difference between those two types of activation processes is the temperature used, which is much higher in case of physical activation. The physical activation with CO_2 or steam allows for porous carbons with unimodal pore size distribution to be obtained, which are perfectly suitable for electrochemical capacitor applications [41]. However, the burn-off factor is very high and therefore the carbon yield of the synthesis is low [42]. Therefore, chemical activation methods have been widely used, as they allow for enriching the surface of the carbon for various types of functionalization. Potassium hydroxide (KOH) is considered to be the most effective chemical activating agent and is widely used for micropore development in the temperature range of 700–800 °C. However, the residues of KOH have to be washed out with acid and, moreover, the carbon yield is rather low [43,44]. Therefore, the whole procedure is considered to be non-sustainable and has limited potential for industrial applications.

It seems that each activation process results in a different pore size distribution. It has been confirmed that the right adjustment of the pore diameter to the size of the ions from the electrolyte remarkably increases the specific capacitance and efficiency of double-layer charging/discharging [45–47]. On one hand, it has been proven that it is mostly the presence of micropores that improves the specific surface area; thus, they play an essential role in the improvement of the specific capacitance of an electrode material [48–51]. On the other hand, mesopores are crucial in terms of a fast charging and good rate handling [52,53]. Therefore, only the balanced combination of both micro and mesopores is reasonable for designing high-energy, high-rate electrochemical capacitors [51]. Tuned parameters of porous carbons might be achieved by applying so-called template-based methods [52,54], which are further distinguished for hard- (H-T) [55–57], soft- (S-T) [58–60] and salt-templating (MeX-T) [61,62] agents.

In the H-T methods, mesoporous silica, often used as template, is fulfilled with a carbon precursor, then annealed and subsequently subjected to acid/base etching [8,63]. This results in the formation of a carbon replica which keeps the hexagonal structure of the silica. Soft-templated techniques attracted great attention due to their simplicity, rapidity and large choice of templates/precursors [58]. In such approach, surfactants able to create hexagonal, cubic or random array moulds are assembled with a phenolic resin carbon source to obtain by simple thermal annealing a 3D carbon material. The materials obtained by the H-T and S-T method are characterized mostly by a mesoporous structure with a fraction of micropores and the pore size depends on the template type, carbon source and processing conditions.

To obtain microporous materials, the novel concept of the template synthesis (salt-templating) has been proposed [64–66]. In this method, inorganic salts are used as templates, which lead to microporosity formation due to the small size of the cations (Li^+, Na^+, K^+, Ca^{2+}, Mg^{2+}, Zn^{2+}) and anions (Cl^-, Br^-). Other parameters that impact the final material properties, besides the kind of cation are template concentration, temperature used, pH or type of the eutectic mixture used for making the synthesis temperature lower. Therefore, in order to obtain micro-mesoporous carbon, both soft- (S-T) and salt-template (MeX-T) approaches have been combined [67,68]. In such a procedure, the soft-template is thermally and fully decomposed, creating a mesoporous carbon structure, whereas the salt-template creates microporosity and can be easily washed out from the sample after the synthesis [67]. It is worth highlighting that the soft- and salt-templating approach ensures high sustainability of the synthesis, where no toxic or hazardous chemical compounds are used, carbon burn is avoided, and moreover, tuneable carbon properties are achieved [67]. High capacitance values (specific and volumetric) balance well the rate capability, slightly worse than for other materials reported, based on graphitic or heteroatom enriched carbons [69,70]. It has to be pointed out, that the concept of applying templated carbons in electrochemical capacitor has already been reported elsewhere [27,71]; however, in the previous reports, the synthesis was unlikely sustainable and complicated.

In this paper, we cover the topics of soft- and salt-template syntheses based on rubidium and caesium chloride salts, which to the best of our knowledge have never been used in this application. The high activity and small size of the solvated cation are beneficial for obtaining a highly porous carbon structure with an optimal pore size. In addition to the physicochemical characteristics of soft- and salt-templated materials, their application in electrochemical capacitors has been explored. The synthesized carbon materials are used as the active material for the electrodes of symmetric electrochemical capacitors. Their high specific surface and moderate density allow for a high specific and volumetric capacitance value to be obtained, compared to commercial activated carbons. Therefore, sustainable electrode materials have been proposed for ECs with an alkaline and neutral electrolytic solution. In this context, it is worth mentioning again, that the synthesis route proposed by us does not involve complicated, multi-step procedures, quite often required for other methods. For instance, NiO and SiO_2 hard templates usually require harsh and dangerous conditions (e.g. using HF or HCl for template removal). Moreover, the precursors used for hard-template infiltration are very often carcinogen (e.g. phenolic resin, polyfurfuryl alcohol) or dangerous (gases such as CH_4, NH_3 are used). In the case of carbon infiltration, Chemical Vapour Deposition (CVD) dangerous procedures must be applied in order to obtain a high-quality and well-dispersed material. Given that, our synthesis route appears to be fully sustainable and very attractive from commercial point of view.

2. Experimental

2.1. Material preparation

Carbon material synthesis involves a one-pot soft-salt template synthesis procedure. Briefly, a carbon source based on phloroglucinol/glyoxylic acid monohydrate, a soft-template, Pluronic® F-127 (Sigma-Aldrich, France) and a chloride inorganic salt-template are dissolved in an ethanol/water mixture to obtain the solution, as described in detail in other studies [67]. Rubidium chloride (RbCl) and caesium chloride (CsCl) salts are proposed for the first time as micropore-creating agents. The ratio of the phloroglucinol carbon source and the salt template was adjusted to 1:2. The NaOH solution is added into the solution in order to obtain a pH of 5 for the reaction mixture, as this allows for the highest surface area of the carbon to be reached [67]. Subsequently, the obtained solution is placed on a Petri dish and pre-dried at room temperature for 12 h in order to evaporate the solvent and to allow the phenolic resin and the template to undergo a self-assembly process. Then the solution is dried at 120 °C for 12 h in order to cross-link the phenolic resin/soft-template. Afterwards, the material is taken from the Petri dish and annealed at 900 °C in an Ar flow for 1 h. After the entire process, inorganic salt is washed out in hot water (80 °C) for the total dissolution of RbCl or CsCl residues. Their high solubility allowed for recovery of the templating agent.

2.2. Physico-chemical characterization

The textural properties of the soft- and salt-templated powders and electrodes were evaluated using N_2 (at 77 K) and CO_2 (at 273 K) sorption isotherms by using ASAP Micromeritics 2420 and 2460. The pristine samples were degassed at 300 °C for 12 h, while for the electrodes the temperature was limited to 100 °C for 24 h to avoid binder degradation. Moreover, a He flow was used before degassing under a vacuum in order to evacuate the impurities from the porosity volume. The Brunauer-Emmett-Teller equation has been used for calculating the specific surface area (SSA) from the linear part of the isotherm at a relative pressure in the 0.01—0.05 range. The Dubinin-Radushkevich (DR) equation has been used for the micropore volume calculation at a relative pressure in the range of 10^{-4} to 10^{-2}. The total pore volume has been determined from the amount of adsorbed N_2 at a relative pressure of 0.95. The pore size distribution (PSD) has been evaluated in the SAIEUS program (Micromeritics) with a 2D-NLDFT heterogenous surface model [72], which to date is the most adequate model for activated carbons.

The structure of the carbon powders was characterized via the X-ray powder diffraction (XRD) technique, using a powder diffractometer D8 ADVANCE A25 from Bruker in Bragg-Brentano reflection geometry $\theta - \theta$. This diffractometer was equipped with the Lynx Eye XE-T high-resolution energy dispersive 1D detector ($CuK\alpha_{1,2}$), allowing for ultra-fast X-ray diffraction measurements. The material's morphology was evaluated via scanning electron microscopy (SEM) analysis using an FEI Quanta 400 scanning electron microscope. The setup was equipped with an energy dispersive analyser (EDX), which was employed to determine the chemical composition of the carbon materials. It has to be mentioned that the composition has been determined for three zones and the paper presents the averaged values. The material structure was investigated with a JEOL ARM-200F transmission electron microscope working at 200 kV.

The Raman analyses for powders and electrode materials were performed at room temperature in a backscattering geometry using a LabRAM BX40 (Horiba Jobin-Yvon) microspectrometer equipped with a He—Ne excitation source (green line, wavelength 532 nm) [73].

2.3. Electrochemical characterization

2.3.1. Electrode preparation

All components, i.e., the synthesized carbon, a polymer binder and carbon soot (90:5:5 wt ratio), were added to a beaker in the presence of ethanol. Carbon black (C65 from Timcal®) was added in order to improve the electrode material conductivity. Then the mixture was continuously stirred at 70 °C in order to evaporate the solvent and prevent decomposition of the polymer binder (polytetrafluoroethylene 60 wt% in H_2O, Sigma Aldrich). The dry composite was then rolled into a thin film, cut into round discs with a diameter of 10 mm and dried in vacuum at 100 °C. The electrode materials prepared in this manner were labelled RbCl-T or CsCl-T for rubidium and caesium chloride, respectively. For comparison purposes, two commercial activated carbons labelled as 507-20 (self-standing cloth from Kynol®) and YP80F (powder from Kuraray) were used. The electrode masses varied between 8.5 mg (CsCl-T, YP80F) and 9.2 mg (507-20). Geometric surface of the electrode was 0.785 cm^2 and the average thickness - 150—200 μm.

2.3.2. Electrochemical evaluation

The electrochemical measurements were performed in symmetric Swagelok® cells with stainless steel current collectors and a Whatman GF/A glass fibre separator (thickness of 260 μm). The applied electrolyte was either 1 mol L^{-1} lithium LiOH or 0.5 mol L^{-1} Li_2SO_4. The cyclic voltammetry at scan rates of 1—100 mV s^{-1}, galvanostatic charging/discharging at 0.1—10 A g^{-1} and the electrochemical impedance spectroscopy in the frequency range of 1 mHz—100 kHz at the selected voltages were performed.

The capacitance values are expressed per single electrode unless stated otherwise. Moreover, for convenient comparisons, in certain cases, the volumetric capacitance has also been presented.

3. Results and discussion

3.1. Physico-chemical analysis of soft- and salt-templated materials

The porosity of the templated carbon powder and electrodes is characterized by nitrogen adsorption, with the textural data summarized in Table 1.

Carbon materials obtained with the new RbCl and CsCl templates exhibited large surface areas of 2077 m^2 g^{-1} and 2556 m^2 g^{-1}, respectively. These values are remarkably higher than those previously obtained with LiCl, NaCl and KCl templates (max. ~1750 m^2 g^{-1}). Such values are also competitive with the surface of commercial activated carbons. CsCl-T offers an extraordinarily high specific surface area, i.e., 2556 m^2 g^{-1}, which results in the high specific surface area of the electrode material (2143 m^2 g^{-1}) prepared with this material. Interestingly, the average pore size is 0.77 and 0.88 nm, which is an optimal size for electrochemical capacitor applications, as already demonstrated [74]. It is noted that the increase in the salt cation size induces a higher surface area and pore size, with CsCl exhibiting the specific surface area close to the theoretical one. For salt- and soft-templated materials, the volume of micropores is very high, i.e., 0.77 and 0.95 cm^3 g^{-1} for RbCl-T and CsCl-T, with a considerable volume of mesopores, i.e., 0.19 and 0.20 cm^3 g^{-1}, respectively. It is also worth mentioning that the average pore size ranges from 0.7 to 0.9 nm.

Taking into consideration the fact that the electrode material components, such as conductive soot (C65) and a polymer binder (PTFE), may decrease the SSA [75], the electrode materials prepared with 90 wt% RbCl-T or CsCl-T have also been analysed. Indeed, we observed a decrease in the SSA. However, the obtained values, i.e., 1764 m^2 g^{-1} and 2143 m^2 g^{-1} are still very satisfactory, especially if compared to electrode materials based on the commercial activated

Table 1
Porosity characteristics of synthesized templated carbons and commercial ones obtained by N_2 adsorption/desorption at 77 K.

Sample name	Specific surface area [$m^2 \cdot g^{-1}$]	V_{micro}<2 nm [$cm^3 \cdot g^{-1}$]	V_{meso}2–50 nm [$cm^3 \cdot g^{-1}$]	L_0 average micropore size <2 [nm]	L_0 average mesopore size 2-50 [nm]
RbCl-T	2077	0.77	0.19	0.77	5.60
CsCl-T	2556	0.95	0.20	0.88	3.86
YP80F	2087	0.80	0.19	1.04	2.81
507–20	1841	0.69	0.00	0.82	2.07
RbCl-T electrode	1764	0.65	0.11	0.81	8.26
CsCl-T electrode	2143	0.81	0.16	0.91	5.15
YP80F electrode	1771	0.68	0.21	1.04	2.85

carbons (YP80F – 1770 $m^2\ g^{-1}$ or 507-20 – 1841 $m^2\ g^{-1}$). This is also worth noting that CsCl-T-based electrodes reveal the highest content of microporosity among all presented materials.

The isotherms and the corresponding pore size distribution for all of the abovementioned electrode materials are shown in Fig. 1. It is important to mention that the decrease in the specific surface area of RbCl-T- and CsCl-T-based electrodes results from clogging the porosity via the presence of the polymer binder and the addition of a low surface area carbon soot. This causes a visible difference in the L_0 parameter for pristine carbon and the electrode material. In fact, for the electrode material, both L_0 values are higher than for pristine, powdered carbons. This indicates that during the electrode formulation process, only the smallest pores are blocked by the binder, as the average values shifts towards higher values.

It can be easily remarked in Fig. 1a that the electrode materials based on templated carbons demonstrate higher SSA values than the commercially available ones. In fact, the sample labelled 507-20 is a highly microporous material and does not reflect any hysteresis loop on the isotherm. It is produced from phenolic resin in a one-step synthesis, and its isotherm overlaps with RbCl-T, which might suggest similar porous properties of both materials. However, RbCl-T reveals a small hysteresis loop resulting from the mesoporosity fraction, which is assumed to guarantee better surface area access at high current regimes. YP80F is produced from the abundant precursor, coconut shells, activated with CO_2.

The implementation of the soft-templating step introduced the mesoporosity fraction in RbCl-T and CsCl-T, which is observed by the presence of hysteresis loop. Given this, it is assumed that the proposed soft- and salt-templated carbons will reveal a high rate capability, which is required for electrochemical capacitors.

Fig. 1b presents the pore size distribution (PSD) for electrode materials. CsCl-T is characterized by the narrowest PSD among all materials. It contains a high fraction of wide micropores and small mesopores. The pore size distribution of RbCl-T-based materials is shifted towards narrower diameters, both in the case of micro- and mesopores. Its PSD almost overlaps with the 507-20 sample, as was already observed in the isotherms. YP80F possess a smaller amount of micropores in comparison to CsCl-T. However, its PSD differs from the other presented materials as the average pore diameter is shifted towards higher values.

CO_2 adsorption was complementarily employed in order to verify the presence of ultra-micropores. A comparison of the electrode material adsorption isotherms is presented in Fig. 1c.

Apart from the differences in the adsorbed molecule dimensions, a higher analysis temperature (273 K) allows for a better adsorbate (CO_2) diffusion in comparison to nitrogen sorption (77 K). Interestingly, the obtained specific surface area values are smaller than those from nitrogen adsorption/desorption for all samples – the pristine carbon material and electrode based on this carbon material. It has been assumed that this difference could be caused by a narrow pressure range used for CO_2 adsorption (vs. N_2 sorption) and by a smaller ultra-micropore fraction (pores <1 nm) compared to regular micropores. Nonetheless, the CO_2 adsorption indicated that the micropore and ultra-micropore volume is higher (1.51 $cm^3\ g^{-1}$) than that from the N_2 analysis (0.95 $cm^3\ g^{-1}$), while the pore size is quite similar. Finally, one can conclude that the synthesized carbons are characterized by well-developed porosity confirmed by two adsorptive techniques.

Interestingly, the conductivity measured for the electrode material indicates that there is no direct correlation between conductivity and the textural properties of the electrode material. Namely, the conductivity was the highest for the RbCl-T (12.1 S m^{-1}), demonstrating almost the same PSD as the material of the lowest conductivity, i.e. 507-20 tissue (8.0 S m^{-1}). Material of the highest S_{BET} (CsCl-T) demonstrated the conductivity of 10.1 S m^{-1}, whereas YP80F – 9.1 S m^{-1}.

The structure of the materials has been assessed via an SEM, TEM micrographs and an XRD study, which are presented in Fig. 2.

The XRD patterns show (Fig. 2a) the absence of (002) peak, indicating the lack of stacked graphitic domains. No other peak (related to the presence of the crystallized structure after synthesis, i.e., salt-template residue) is observed, suggesting that synthesized carbons are free from impurities. This confirms that salt-template recovery is possible and highly efficient, as no traces of the crystal structure are found in the final material. Certainly, a broad (100) peak at 43 $2\Theta^o$ cannot be neglected but instead suggests the disordered graphitic domains in the material in the form of long carbon chains. The TEM images support this statement as mostly the microporous structure is visible. Moreover, one should remark that the synthesized material is homogenous throughout the entire volume. The SEM micrographs, Fig. 2b–e, present various morphologies of the electrode materials. At first glance, the various particle sizes of the RbCl-T-, CsCl-T- and YP80F-based material are seen. The particle sizes range from 20 to 75 μm for RbCl-T, 10–50 μm for CsCl-T, 3–7 μm for YP80F. Therefore, it is worth highlighting that commercial activated carbon reveals a more uniform and smaller particle size. 507-20 is interlaced with wires with a diameter of 7 μm. For both the soft- and salt-templated methods graphene-like sheets are visible. 507-20 is composed of carbon fibres without any additives. As graphene-like planes draw our attention, the HRTEM for the soft- and salt-templated materials have been performed with the results presented in Fig. 2f–g. The homogenous structure for both samples is noticeable and graphene-like structures have been found. It can be concluded that the graphene-like planes are not stacked to form many layers on the graphitic domains, therefore explaining the absence of the (002) peak on the XRD.

In addition to the structure analysis from the XRD, SEM and TEM, the Raman spectra have been recorded to gain more insight into the local structure, i.e., the disordered degree, the type of carbon-carbon and the carbon-hydrogen bonds. Thus, in Fig. 3 the

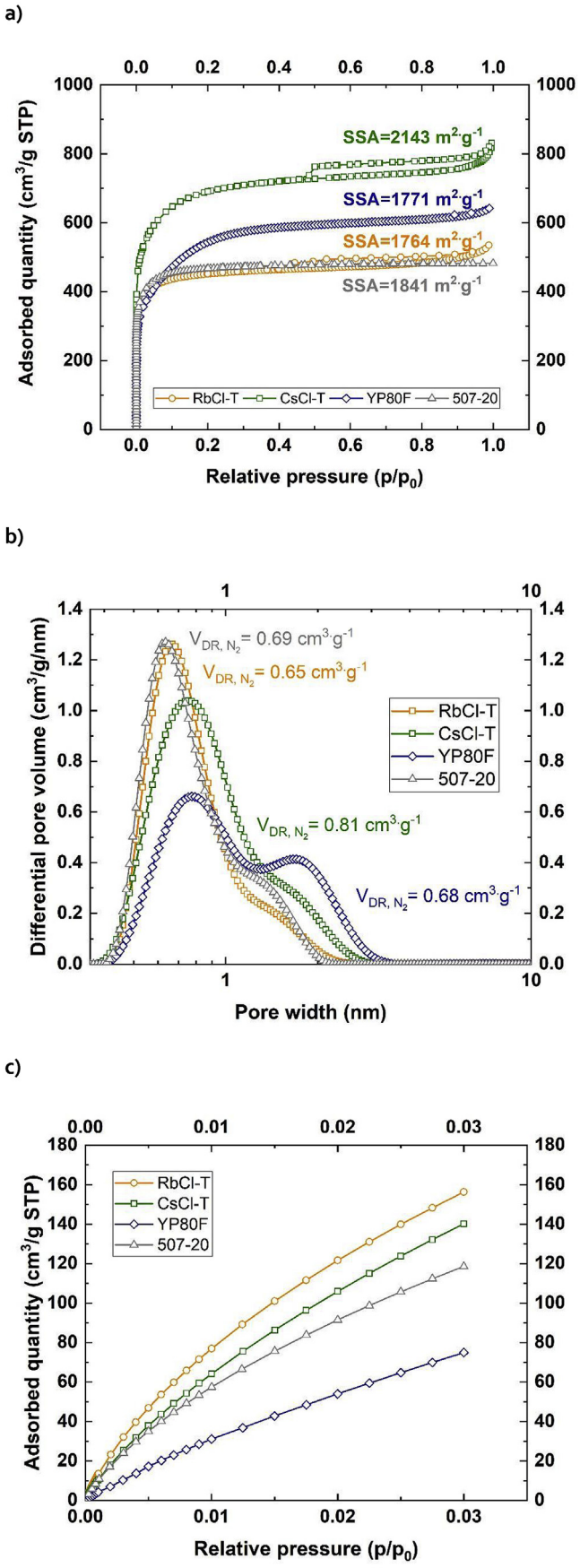

Raman spectra with deconvoluted peaks are presented for RbCl-T (**a**) and CsCl-T (**b**).

The I_D/I_G ratio calculated from the intensity of the experimental spectra is equal to 0.88 and 0.90 for RbCl-T and CsCl-T. However, taking the area ratio between the D and G bands into account, it was determined that for RbCl-T this ratio is equal to 2.71, whereas for CsCl-T it is 2.16, indicating that the comparison between the intensity values for activated carbons can sometimes give misleading information. For the calculated I_D/I_G ratio (0.88 and 0.90), it is shown that the materials are characterized by more graphitic domains in a carbon matrix. However, the values 2.71 and 2.16 calculated from the ratio of the area under the curves indicate that the materials are disordered, which is in accordance with the XRD and TEM results. Moreover, the materials that are composed of various allotropic forms of carbon require deconvolution of the Raman spectra, as the information about the surface oxidation state or surface chemistry might be thus obtained. The recorded "centres of gravity" for the D and G band peaks are 1342 cm^{-1} and 1590 cm^{-1} (RbCl-T) and 1349 cm^{-1} and 1584 cm^{-1} (CsCl-T), whereas for an ideal graphitic material it is usually 1353 cm^{-1} and 1581 cm^{-1}, respectively [76–79]. This shows that the spectra recorded for synthesized carbons are shifted towards higher values of the Raman shift, indicating deviation from the ideal graphitic structure.

Comparing both types of carbons, particular similarities can be listed. The C=C stretching vibration has the same reflection for both spectra. The intensities of the deconvoluted G-band peaks are the same for both carbons. Nonetheless, the D′-band is much less pronounced for the CsCl-T sample. The presence of broad peaks in the Raman shift from 2500 to 3000 cm^{-1} indicates a high amount of sp^2 carbon, which results in a good electrical conductivity of soft- and salt-templated materials.

Because the oxygen content has a crucial influence on the electrochemical performance, prior to conducting an electrochemical comparison, an EDX was performed on the materials, with the results presented in Table 2.

As can be seen in Table 2, all carbon materials have similar carbon and oxygen contents, i.e., 92 at% and ca. 8 at%, respectively. For commercial carbons, some impurity traces (up to 0.05 at%) have been found, such as silica and potassium. These are most likely the residues from the manufacturing process and/or synthesis route. Given that, it has been assumed that the content of other alkali metals in the synthesized material is negligibly low, as it was not indicated by the EDX. However, it has to be pointed out that the level of impurities does not suggest any significant content of them; their presence should not be excluded and neglected, essentially in the case of some peculiar performance observed.

3.1.1. Electrochemical analysis

The prepared carbon materials were tested with two electrolytes, i.e., 1 mol·L^{-1} lithium hydroxide (LiOH) and 0.5 mol·L^{-1} lithium sulphate (Li_2SO_4). Such electrolytes were selected because of their high conductivity and pH values. 1 mol L^{-1} lithium hydroxide is a strongly alkaline solution with a high conductivity of 155 mS cm^{-1}. In contrast, lithium sulphate is neutral with a moderate conductivity (40 mS cm^{-1}). Furthermore, they can be easily applied in commercial aqueous ECs, since no noble metals are required for the current collector.

The LiOH solution is characterized by a high conductivity and thus allows for the preliminary tests in the electrochemical

Fig. 1. Nitrogen adsorption/desorption isotherms recorded at 77 K (a); pore size distribution (b); CO_2 adsorption isotherms of electrode materials based on RbCl-T, CsCl-T, YP80F, and 507-20.

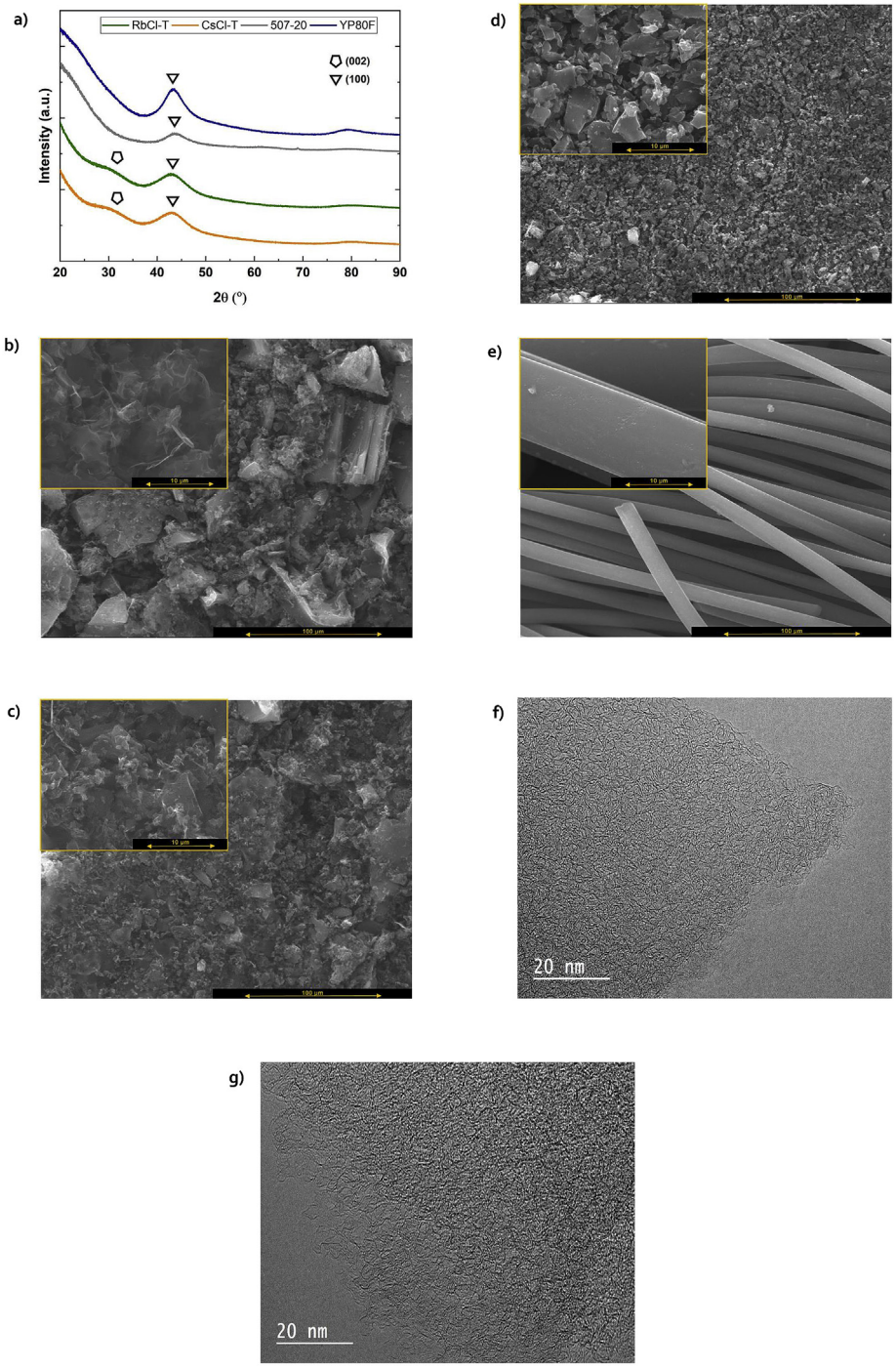

Fig. 2. Electrode material based on RbCl-T, CsCl-T, YP80F and carbon cloth 507-20 characterization: a) XRD pattern; SEM micrographs for RbCl-T (b), CsCl-T (c), YP80F (d) and 507-20 (e); TEM images for RbCl-T (f) and CsCl-T (g).

capacitor application. An aqueous solution of Li_2SO_4 is widely accepted as a neutral electrolyte, allowing for high capacitor operating voltage to be achieved.

The cyclic voltammetry and constant current load profiles recorded for the electrochemical capacitors based on RbCl-T and CsCl-T with a 1 mol·L^{-1} LiOH solution are presented in Fig. 4.

As seen from the cyclic voltammetry and galvanostatic charging/discharging, both ECs performed similarly to one another from a qualitative and quantitative point of view. The cyclic voltammograms have a rectangular-like shape, suggesting a good surface area access and satisfactory conductivity of the electrode materials. The curves almost overlap one another for RbCl-T and CsCl-T. The specific capacitance values calculated from the discharge curve (1 A g^{-1}) are 175 and 187 F g^{-1} for RbCl-T and CsCl-T, respectively. Both values are found to be high in comparison to the literature data [80–85]. Moreover, the energetic efficiency of the charging/discharging process is high, i.e., 99% and 96% for RbCl-T- and CsCl-T-based ECs, respectively. The galvanostatic charging/discharging curves reveal a pure EDL performance, as no deviation from the triangular shape has been found. Moreover, even for a relatively

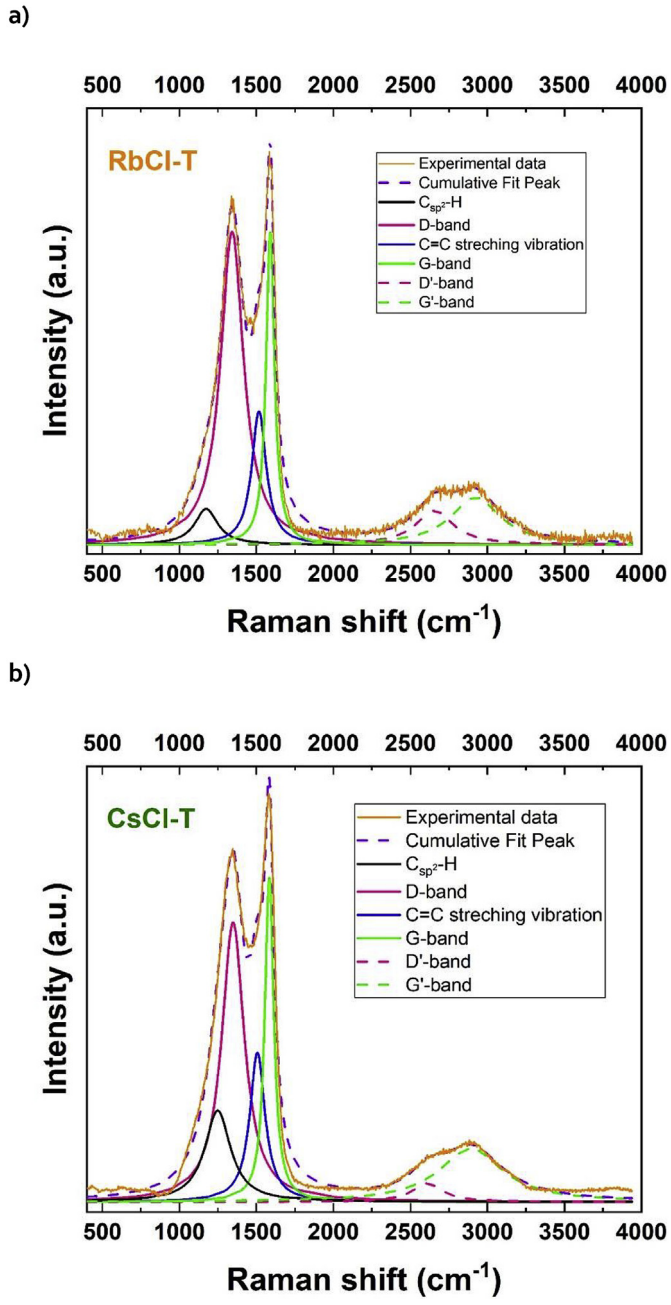

Fig. 3. Raman spectra recorded for the RbCl-T (a) and CsCl-T (b) samples, with the peaks deconvoluted from the experimental line.

Table 2
Atomic composition of carbon materials as revealed by the EDX technique.

Sample name	C, at%	O, at%	Si, at%	K, at%	Total, at%
RbCl-T	91.62	8.38	–	–	100
CsCl-T	92.75	7.25	–	–	100
YP80F	92.10	7.85	0.05	–	100
507–20	92.30	7.65	–	0.05	100

high current load, i.e., 1 A g^{-1}, the ohmic drop is negligible. To verify the rate handling of RbCl-T- and CsCl-T-based devices, the specific capacitance of the electrochemical capacitors vs. the current density is presented in Fig. 4c. Initially, at 0.1 A·g^{-1} high specific capacitance values were recorded: 206 F g^{-1} and 216 F g^{-1} for RbCl-

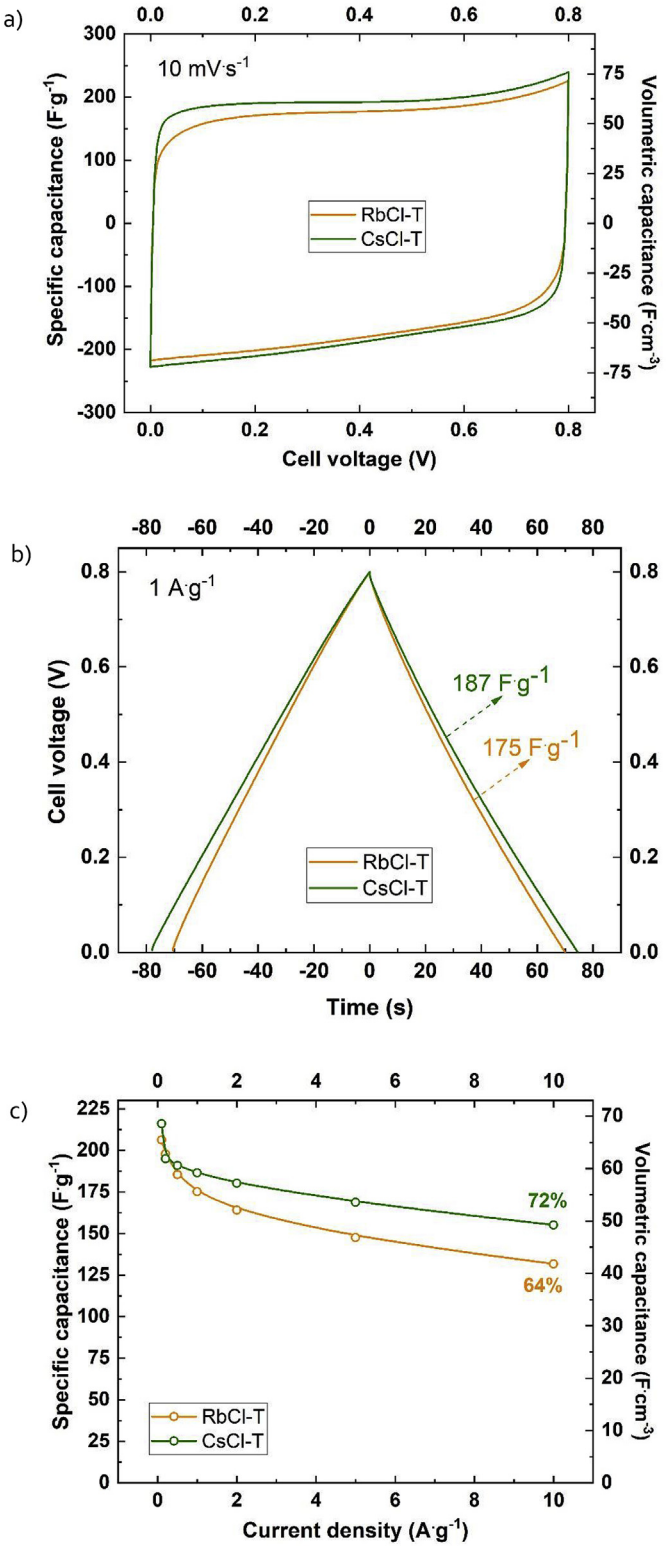

Fig. 4. Electrochemical performance of RbCl-T- and CsCl-T-based EDLC with 1 mol·L^{-1} LiOH as an electrolyte: a) cyclic voltammetry at 10 mV s^{-1}; b) galvanostatic charging/discharging with current density 1 A g^{-1}; c) specific and volumetric capacitance vs. current density.

T and CsCl-T, respectively. Moreover, it must be noted that even at a high current load, i.e., 10 A g^{-1}, the recorded specific capacitance is high, i.e., 132 F g^{-1} (for RbCl-T) and 155 F g^{-1} (for CsCl-T). These values state a 64% and 72% rate handling. Therefore, ECs based on RbCl-T and CsCl-T are capable of handling high current loads, suggesting that these materials are perfectly suitable for high power electrode materials.

The ECs with 1 mol L^{-1} LiOH solution based on RbCl-T and CsCl-T are characterized by high specific capacitance values, good surface area access and very small resistivities. Thus, after the successful implementation of synthesized materials with a highly conductive electrolytic solution (155 mS cm^{-1}), electrochemical capacitors with a sulphate-based electrolyte (40 mS cm^{-1} for 0.5 mol·L^{-1} Li_2SO_4) have been built in order to verify the application of such a material in an environment-friendly medium of moderate conductivity. Fig. 5 presents data collected in the voltage range 0 ÷ 0.8 V for ECs based on RbCl-T, CsCl-T, YP80F and 507-20 with 0.5 mol L^{-1} Li_2SO_4.

It can be observed that symmetric ECs are characterized by a very satisfactory rate handling calculated from the potentiodynamic mode (>50%). Moreover, the specific capacitance calculated either per mass or volume of the electrode is doubled when soft- and salt-templated materials are used in comparison to commercial ACs. The best recorded rate handling during CV tests in the scanning rate of 1–100 mV s^{-1} is for YP80F-based EC. However, considering rate handling calculated from the galvanostatic mode, the presence of mesopores is crucial in order to efficiently operate at high current regimes. The highly microporous 507-20 material reveals the worst electrochemical performance: only 29% of initial specific capacitance is available when a 10 A g^{-1} current density is applied. CsCl-T-based EC exhibits the highest rate handling (63%) at 10 A g^{-1}. Furthermore, the specific capacitance calculated from the potentiodynamic and galvanostatic modes are in accordance, i.e., almost 160 F g^{-1} (50 F cm^{-3}) for CsCl-T, 146 F g^{-1} (45 F cm^{-3}) for RbCl-T, 100 F g^{-1} (30 F cm^{-3}) for YP80F and 90 F g^{-1} (27 F cm^{-3}) for 507-20 at 0.1 A g^{-1}. All tested systems exhibit negligible ohmic drops, which can also be seen from the low ESR value at the Nyquist plot, <1 Ohm. Hence, the impedance spectroscopy recorded at 0.8 V reveals the lack of a semicircle, indicating a good contact between the electrode material and stainless-steel current collector. However, two characteristic points could be distinguished: the equivalent series resistance (ESR) at 100 kHz and the equivalent distributed resistance (EDR), obtained from the extrapolation of the impedance spectra at a lower frequency. The ESR is equal to 0.66 Ohm for RbCl-T-based EC, proving that the adhesion of the electrode material to the current collector is satisfactory (negligible contact resistance) and only the electrolyte is responsible for the current flow through the cell (electrolyte resistance). The recalculation with the distance between the current collectors and their surface reflects the calculated conductivity being equal to 40 mS cm^{-1}, i.e., the conductivity of the electrolytic solution itself. EDR (2.33 Ohm for RbCl-T), however, is the sum of ESR (0.66 Ohm) and the ionic solution resistance “dissipated” within the pore volume. Thus, it could be adjusted/affected by the thickness of electrodes as well as the micro/mesopore volume in the electrode material. The EDR values are in the range of 2–2.5 Ohm for all studied ECs. In the low-frequency range, the curves slightly deviate from their ideal capacitive behaviour, which results from a porous structure of the electrode materials. Therefore, in order to compare the ECs, a more detailed specific capacitance has been calculated in the frequency range of 1 mHz–100 kHz, both at 0 V and 0.8 V, (Fig. 5d–e). The specific capacitance values are slightly higher when the voltage is maintained at 0.8 V rather than at 0 V, but the differences are negligible. The shapes of the curves vary for soft- and salt-templated materials only, while for YP80F and 507-20 they almost overlap one another. This could be related with mesoporosity contribution in the energy storage mechanism. The highest specific capacitance at 1 Hz, so 1 s of charging/discharging has been reached by the CsCl-T-based EC (62/66 F g^{-1} at 0 V/0.8 V).

The high-rate capability of synthesized materials has been proven in alkaline and neutral media. Thus, in the last step, the maximum voltage window has been verified for the electrochemical capacitor based on the CsCl-T electrode material (as it was the most promising one) in the 0.5 mol L^{-1} Li_2SO_4 electrolytic solution. The cyclic voltammetry with a scan rate of 2 mV s^{-1} and galvanostatic charging/discharging with a current density of 0.1 A g^{-1} has been performed in a sequence 0 ÷ 1.8 V with an increasing voltage range (0.1 V) from 0.8 V up to 1.8 V, presented in Fig. 6.

Additionally, 1.5 V has been selected as the maximum operational voltage window based on the calculation of energetic and coulombic efficiency from both potentiostatic and galvanostatic modes. After exceeding 1.5 V, the energy provided to the system during charging is much higher than the energy released during discharging. Moreover, at 1.5 V, the cyclic voltammogram is characterized by a quasi-rectangular shape. Higher vertex voltages result in a deviation from the ideal capacitive behaviour for corresponding scans; the redox peaks become increasingly pronounced for voltages higher than 1.5 V, which are most likely caused by hydrogen sorption on the negative electrode.

Therefore, a comparison of ECs in the maximum voltage has been made. Fig. 7 represents the cyclic voltammetry profiles (at 5 mV s^{-1}) and the galvanostatic charging/discharging profile at 1 A g^{-1}. Moreover, the specific capacitance values calculated from the potentiodynamic and galvanostatic modes have been presented.

All ECs exhibit very good rate handling, visible in the rectangular CV shape at 5 mV s^{-1} (Fig. 7a). At 1.5 V a negligible difference can be found between the YP80F- and 507-20-based ECs. For CsCl-T, the highest specific capacitance has been recorded (almost twice higher at low scanning rates, and +50% at high and moderate, i.e., >20 mV s^{-1}) compared to the commercial activated carbons. Fig. 7b shows the galvanostatic charging/discharging profiles at a relatively high current density, 1 A g^{-1}. All systems are characterized by a small ohmic drop, which is in accordance with studies performed at 0.8 V. Moreover, the curves resemble an ideal isosceles triangle, which confirms the very good coulombic efficiency of >90%. The energetic efficiency is approximately 85% for all samples for an applied voltage of 1.5 V. Fig. 7c–d presents the specific capacitance values calculated from the galvanostatic charging/discharging and cyclic voltammetry, respectively. In each case, the CsCl-T-based ECs reveal the highest specific capacitance but the worst or moderate rate handling. Thus, a system operating at 10 A g^{-1} exhibit 58% of the initial specific capacitance value, which is almost 50% more than that for YP80F and 507-20. Therefore, novel electrode materials are attractive for energy storage applications. It is worth reminding that the novel synthesis method presented within this paper is fully sustainable, eco-friendly and moreover gives an opportunity to re-use the salt-template used during the synthesis, which influences its overall cost and applicability.

To evaluate the performance of the CsCl-T material as a component of the ECs, a final comparison with 507–20 and YP80F has been presented in Fig. 8 in a so-called Ragone plot.

It is noted that the system based on soft- and salt-templated electrode materials gains almost 75% of the energy density calculated for the same current densities compared to the other carbons (16.7 Wh·kg^{-1} vs. 9.5 Wh·kg^{-1}). Moreover, an almost constant energy profile vs. power confirms that there is an excellent capacitive performance even at high voltages. An increase in the operating voltage from 0.8 V to 1.5 V improves the energy density

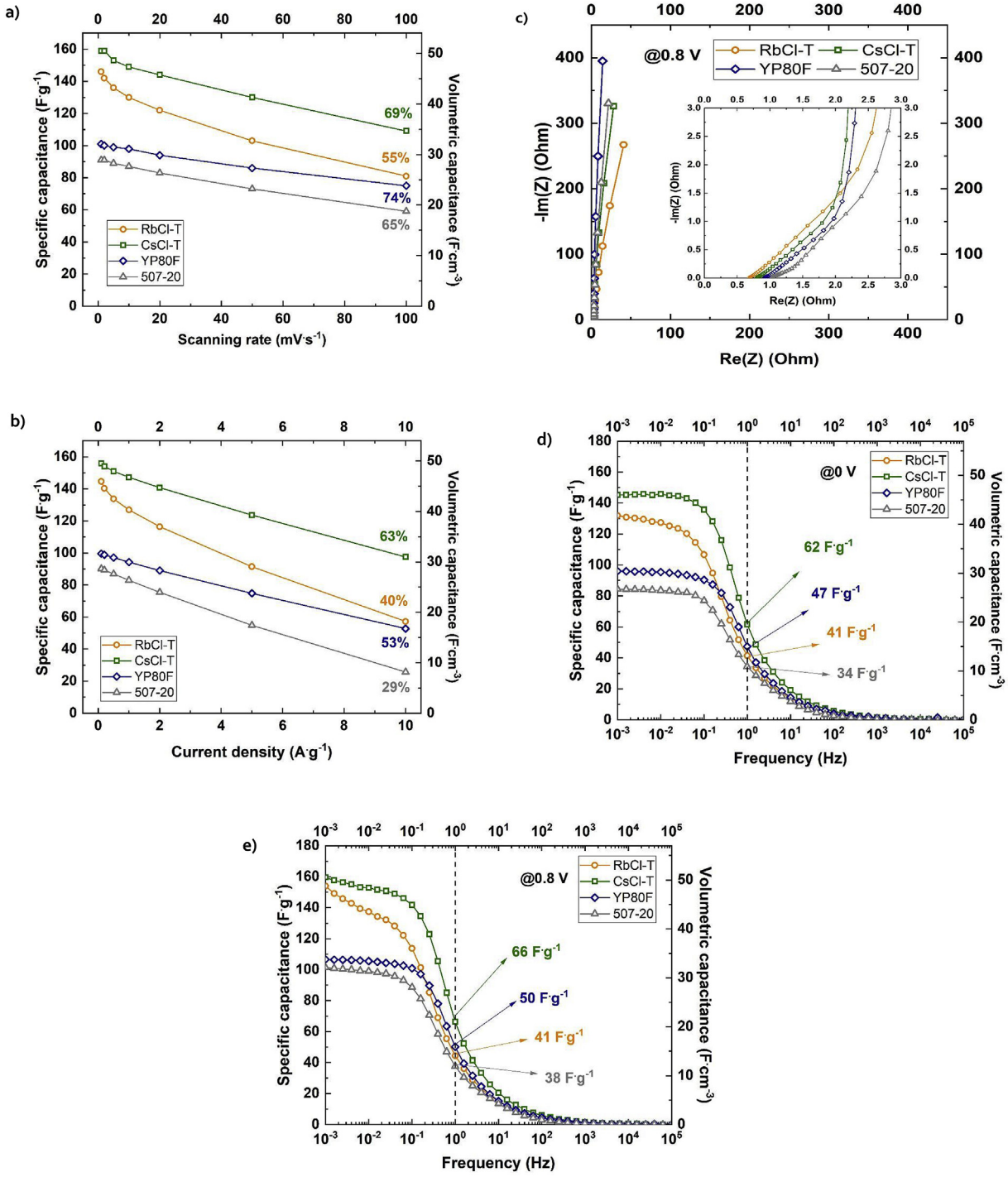

Fig. 5. Electrochemical capacitor based on an RbCl-T, CsCl-T, YP80F, 507-20 electrode material operating with 0.5 mol·L^{-1} Li_2SO_4: a) specific capacitance vs. scanning rate; b) specific capacitance vs. current density; c) electrochemical impedance spectroscopy recorded at 0.8 V; d) specific capacitance vs. frequency at 0.0 V; e) specific capacitance vs. frequency at 0.8 V. The percent values represent the capacitance retention.

value from 3.5 Wh·kg^{-1} to 16.7 Wh·kg^{-1} (+350%) for CsCl-T-based ECs.

The long-term stability at the capacitors voltage of 1.5 V has been determined by so called floating test. Briefly, the capacitors have been subjected to several voltage-holding periods (2 h). After each floating sequence, the capacitance values have been determined by the galvanostatic method. For comparison purposes, the same test has been applied to the capacitors built with 507−20 and YP80F carbon materials. The results are presented in Fig. S1.

Apart from regular pattern for the capacitor operating with 507−20 electrodes, one can note that for the systems operating with CsCl-T and YP80F carbons, so-called “cell conditioning” occurs during initial 30 h of the floating test. Interestingly, for YP80F carbon, the capacitance slightly increases. In this case, two different factors might be at the origin of such a peculiar performance. Firstly, the electrolyte might still be penetrating the (highly

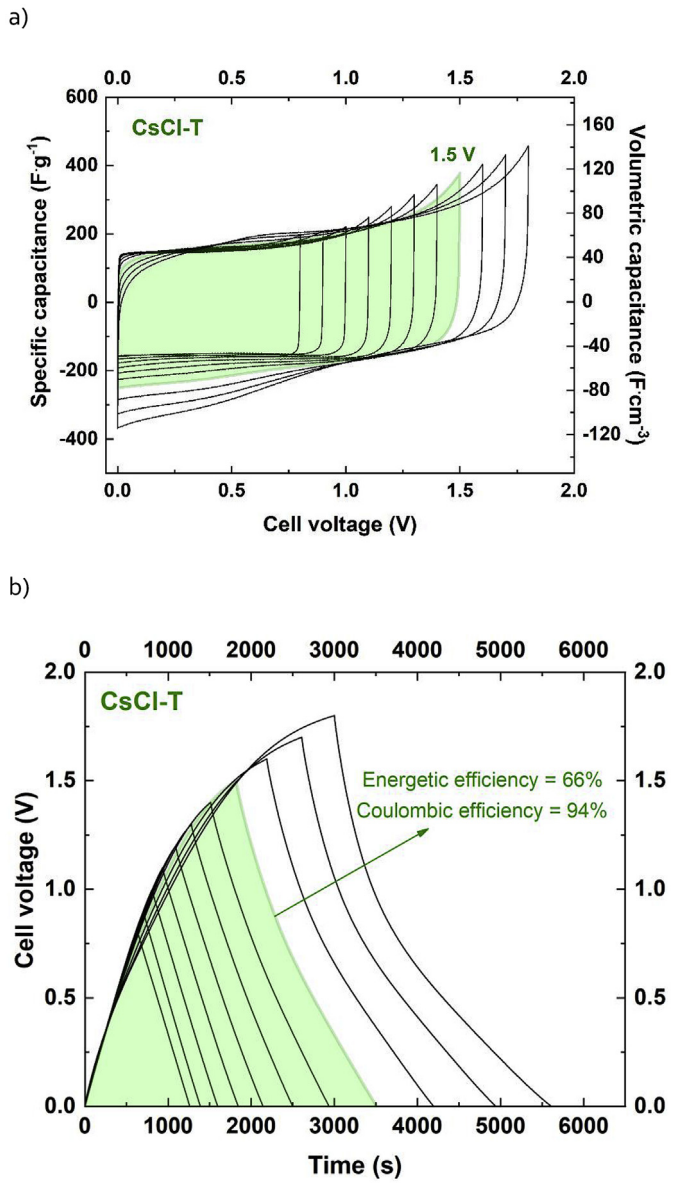

Fig. 6. Extension of the voltage window for EC based on the CsCl-T electrode material with 0.5 mol·L^{-1} Li_2SO_4: a) cyclic voltammetry at 2 mV s^{-1} scan rate; b) galvanostatic charging/discharging at 0.1 A g^{-1}.

microporous) carbon electrode bulk, resulting in the development of the electrode/electrolyte interface. Secondly, as the capacitor voltage exceeds water decomposition voltage, pseudocapacitive hydrogen storage cannot be neglected [86–88]. This might result in the incremental capacitance increase; however, recent reports suggest that this effect might be detrimental in the long-term perspective [89–91].

For CsCl-T based cell, the capacitance initially drops (first 20 h of the floating test) but then is being recovered. In this case, it is assumed that the capacitance drop comes from the electrode potential-range adjustment under high voltage-conditions. Namely, it is expected that potential range values during purely capacitive operation must be different than for conditions enforced by elevated voltage. Taking into account strictly microporous character of the CsCl-T carbon electrode, a certain time is required to accommodate the ions in the respective pores. Capacitance increase after conditioning time suggests that ions are successfully stored inside the pores. However, one should not neglect the contribution from hydrogen electrosorption in this case as well. In this case, the capacitance variation observed, originate rather from mechanical disintegration of the electrode (observed after cell disassembling) than carbon oxidation. This might suggest that further optimisation in terms of binder might still improve the overall performance.

Taking into account the results herein obtained, it can be claimed that the proposed soft- and salt-templated carbon, combining the high surface area, the optimal micropore size, the good balance between micro and mesopores and the conductive structure, is suitable for high-voltage electrochemical applications. To understand the reason behind such a good performance compared to activated carbons, the following explanation based on material characteristics can be proposed. As mentioned in the introduction, many factors can impact the electrochemical performance, and those related to the material porosity, structure and surface chemistry are the most important ones. The structure of the materials (graphitization level) has a direct link with the electronic conductivity of the materials and an influence on the surface area access. As the structures of the soft- and salt-templated and the commercial carbon materials were found to be similar (Raman/XRD analyses), the influence of this parameter can be considered negligible. Regarding the surface chemistry, the presence of oxygen functional groups is known to induce the hydrophilic behaviour of the materials and possible redox reactions with the electrolyte, which may improve the material's (pseudo)capacitance. However, the EDX technique revealed almost the same amount of oxygen in all materials. Hence, its impact on the performance will be the same for all materials. The last important carbon characteristic is the porosity, where both the specific surface area and pore size/volume are of prime importance. A high specific surface area allows the adsorption of the electrolyte ions in the pores and ensures a high capacitance. It is the case of the CsCl-T material that exhibits the highest surface area (2576 m^2 g^{-1} or 2143 m^2 g^{-1} for an electrode material with 90 wt% of synthesized carbon) among the materials, resulting in the highest capacitance (160 F g^{-1} at 0.1 A g^{-1} in 0.5 mol L^{-1} Li_2SO_4). Nevertheless, the pore size must match the electrolyte ion size, which is the case for all materials since they have an average pore size of approximately 0.8–0.9 nm, which is ideal for such applications. Therefore, the high capacitance of the templated carbons is derived from their high specific surface area given by pores with optimal size. However, the rate capability behaviour was found to be very good (72% and 64% for CsCl-T and RbCl-T in 1 mol L^{-1} LiOH and 69% and 55% for CsCl-T and RbCl-T in 0.5 mol L^{-1} Li_2SO_4, respectively) compared to the commercial carbons, particularly (65% in 0.5 mol L^{-1} Li_2SO_4). It is worth mentioning that the last one is a purely microporous material without mesopores (V_{meso} = 0.00 cm^3 g^{-1}), contrary to the CsCl-T material, which displays a mesopore volume, V_{meso} of 0.20 cm^3 g^{-1}. This suggests that mesopores are responsible for the high rate capability of templated materials by allowing a good/fast access of the electrode surface area for the electrolyte throughout the material. To conclude, the high capacitance, good rate capability and energy density of the templated materials are ascribed to a proper combination of several features, i.e., a high surface area, optimal micropore size, good balance between micro and mesopores and a conductive structure.

To prove the abovementioned statement, a Ragone plot has been recalculated from the impedance spectra recorded at an elevated voltage, as presented in Fig. S2. The energy and power were obtained from the capacitance values calculated with imaginary part of the impedance at elevated voltage. The time (for power estimation) has been recalculated from the frequency value.

It is worth highlighting that the energy output prediction and

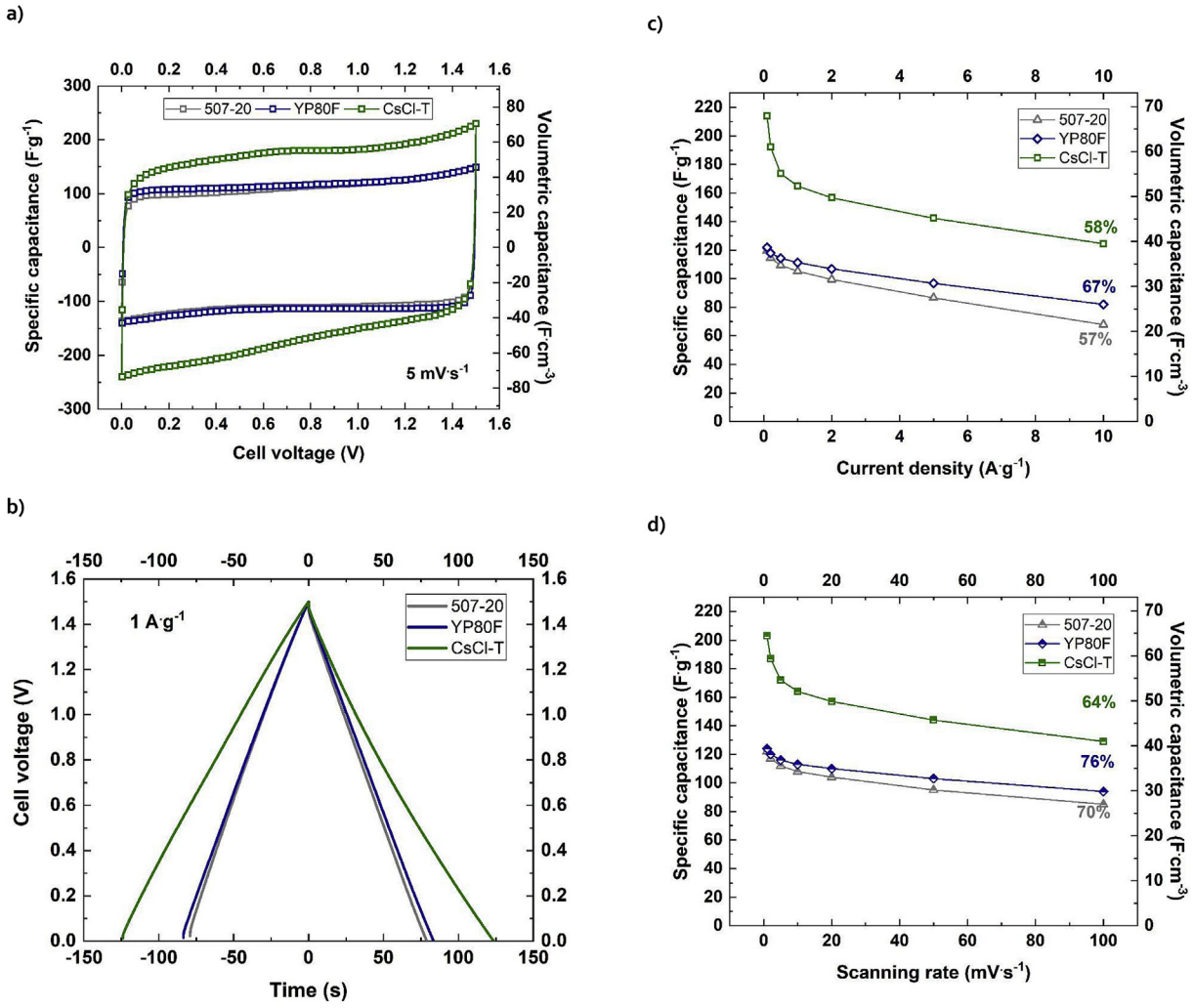

Fig. 7. Comparison of ECs based on CsCl-T, 507-20 and YP80F at 1.5 V: a) cyclic voltammetry at 5 mV s^{-1}; b) galvanostatic charging/discharging at 1 A g^{-1}; c) capacitance retention vs. current density; d) capacitance retention vs. scanning rate. Electrolyte solution 0.5 mol·L^{-1} Li_2SO_4.

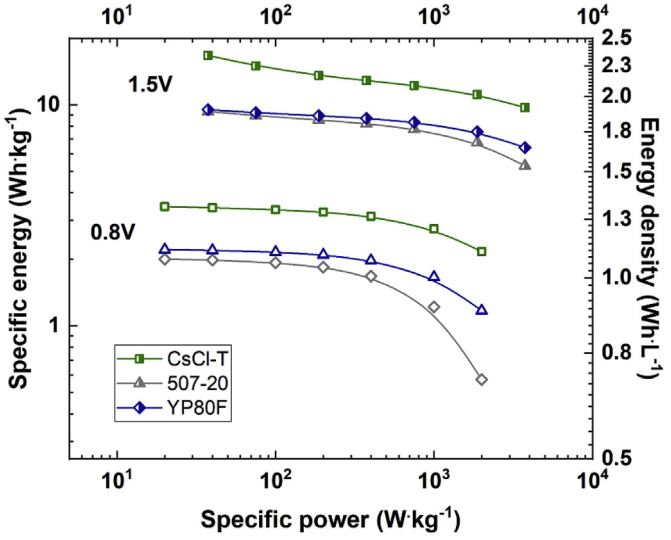

Fig. 8. Ragone plot of ECs working at 0.8 V and 1.5 V with 0.5 mol L^{-1} Li_2SO_4 electrolytic solution and three various electrode materials, i.e., CsCl-T, 507-20, and YP80F.

values obtained from the galvanostatic mode are somehow in accordance with one another. From such a recalculation, it can be indicated that at a low voltage a soft- and salt-templated material reveals the highest rate-capability in comparison to commercial samples. However, it has to be clearly stated that the energy and power calculated from the electrochemical impedance spectroscopy technique should not be considered as absolute values; quite often these values might be over/underestimated as they are calculated for very small voltage amplitudes and might not reflect an overall performance within considered operating voltage range [92]. Thus, they might serve for comparative purposes only.

4. Conclusions

1) The soft- and salt-template approach was explored in this work in order to obtain porous carbons based on novel rubidium chloride and caesium chloride salt-templates. The obtained materials combined a high surface area (2077 and 2556 m^2 g^{-1} for RbCl-T and CsCl-T, respectively), a high microporosity with an optimal uniform pore size (~0.8 nm) that is able to adsorb ions quickly and a certain degree of mesoporosity to ensure fast access of the electrode surface area for the electrolyte.

2) The structure was found to be disordered but with enough sp^2 carbon atoms to ensure a good conductivity for the material, and the surface chemistry reveals oxygen groups useful for wettability with the electrolyte.
3) The application of these carbons in electrochemical capacitors revealed a specific capacitance at 1 A g^{-1} of 175 F g^{-1} and 187 F g^{-1} in 1 mol L^{-1} LiOH for RbCl-T- and CsCl-T-based electrode materials, respectively.
4) The specific capacitances of the materials in a 0.5 mol L^{-1} Li_2SO_4 neutral electrolyte were 127 F g^{-1} (RbCl-T) and 147 F g^{-1} (CsCl-T) at 1 A g^{-1}. The rate handlings were at the level of 40% and 63% for RbCl-T and CsCl-T-based carbons, respectively. Therefore, the CsCl-T material has been found to be a more suitable electrochemical capacitor than RbCl-T.

The overall performance of ECs CsCl-T-based with 0.5 mol L^{-1} Li_2SO_4 were found to be better than those for ECs built with commercial activated carbons. The specific capacitance was higher by 50% (156 F g^{-1}) compared to the other cells (90 F g^{-1} for the carbon tissue and 100 F g^{-1} for YP80F). A maximum voltage of 1.5 V was achieved in the neutral electrolyte, resulting in a significant high energy density, i.e., 16.7 Wh·kg^{-1} at 30 W kg^{-1} of the specific power for ECs with CsCl-T electrode material compared to 9.5 Wh·kg^{-1} for commercial activated carbons. The highest capacitance has been preserved during 120 h of voltage-holding test at capacitor voltage of 1.5 V.

Therefore, this sustainable synthesis method presented herein allows for porous carbon materials with suitable textural and structural characteristics to be obtained. A good electrochemical performance in terms of the specific capacitance, rate handling, and high voltage has been demonstrated.

Acknowledgements

The authors acknowledge the French Ministry for Europe and Foreign Affairs (MEAE) and the French Ministry of Higher Education, Research and Innovation (MESRI) and Polish Ministry of Science and Higher Education through PHC POLONIUM PROJECT N37783YJ.

The European Research Council is acknowledged for their financial support within the Starting Grant project (GA 759603) under European Unions' Horizon 2020 Research and Innovation Programme.

The authors thank the French National Research Agency for its support through the Labex STORE-EX project (ANR-10LABX-76-01).

We thank Loïc Vidal, Stephan Knopf and Jean-Marc Le Meins for performing the TEM, SEM/EDX and XRD measurements via the technical IS2M platforms.

Appendix A. Supplementary data

Supplementary data to this article can be found online at https://doi.org/10.1016/j.electacta.2020.135788.

References

[1] A. Burke, R&D considerations for the performance and application of electrochemical capacitors, Electrochim. Acta 53 (2007) 1083–1091.
[2] J.R. Miller, A.F. Burke, Electrochemical capacitors: challenges and opportunities for real-world applications, Electrochem. Soc. Interf. 17 (2008) 53–57.
[3] J. Ho, T.R. Jow, S. Boggs, Historical introduction to capacitor technology, IEEE Electr. Insul. Mag. 26 (2010) 20–25.
[4] A.K. Shukla, A. Banerjee, M.K. Ravikumar, A. Jalajakshi, Electrochemical capacitors: technical challenges and prognosis for future markets, Electrochim. Acta 84 (2012) 165–173.
[5] C. Cader, P. Bertheau, P. Blechinger, H. Huyskens, C. Breyer, Global cost advantages of autonomous solar-battery-diesel systems compared to diesel-only systems, Energy Sustain. Dev. 31 (2016) 14–23.
[6] A. Chu, P. Braatz, Comparison of commercial supercapacitors and high-power lithium-ion batteries for power-assist applications in hybrid electric vehicles I. Initial characterization, J. Power Sources 112 (2002) 236–246.
[7] K. Fic, A. Platek, J. Piwek, E. Frackowiak, Sustainable materials for electrochemical capacitors, Mater. Today 21 (2018) 437–454.
[8] M. Inagaki, H. Konno, O. Tanaike, Carbon materials for electrochemical capacitors, J. Power Sources 195 (2010) 7880–7903.
[9] L. Dai, D.W. Chang, J.B. Baek, W. Lu, Carbon nanomaterials for advanced energy conversion and storage, Small 8 (2012) 1130–1166.
[10] F. Beguin, V. Presser, A. Balducci, E. Frackowiak, Carbons and electrolytes for advanced supercapacitors, Adv. Mater. 26 (2014) 2219–2251, 2283.
[11] M. Winter, R.J. Brodd, What are batteries, fuel cells, and supercapacitors? Chem. Rev. 104 (2004) 4245–4270.
[12] R. Kötz, M. Carlen, Principles and applications of electrochemical capacitors, Electrochim. Acta 45 (2000) 2483–2498.
[13] A. Gonzalez, E. Goikolea, J.A. Barrena, R. Mysyk, Review on supercapacitors: technologies and materials, Renew. Sustain. Energy Rev. 58 (2016) 1189–1206.
[14] H. Marsh, F. Rodríguez-Reinoso, Activated Carbon (Origins), Activated Carbon2006, pp. 13-86.
[15] E. Frackowiak, K. Metenier, R. Pellenq, S. Bonnamy, F. Beguin, Capacitance properties of carbon nanotubes, Electronic Properties of Novel Materials - Science and Technology of Molecular Nanostructures, vol. 486, 1999, pp. 429–432.
[16] P. Simon, Y. Gogotsi, Materials for electrochemical capacitors, Nat. Mater. 7 (2008) 845–854.
[17] E. Raymundo-Pinero, M. Cadek, M. Wachtler, F. Beguin, Carbon nanotubes as nanotexturing agents for high power supercapacitors based on seaweed carbons, ChemSusChem 4 (2011) 943–949.
[18] G. Lota, K. Fic, E. Frackowiak, Carbon nanotubes and their composites in electrochemical applications, Energy Environ. Sci. 4 (2011) 1592–1605.
[19] G. Centi, S. Perathoner, Carbon nanotubes for sustainable energy applications, ChemSusChem 4 (2011) 913–925.
[20] Y. Zhai, Y. Dou, D. Zhao, P.F. Fulvio, R.T. Mayes, S. Dai, Carbon materials for chemical capacitive energy storage, Adv. Mater. 23 (2011) 4828–4850.
[21] Y. Zhu, S. Murali, M.D. Stoller, K.J. Ganesh, W. Cai, P.J. Ferreira, A. Pirkle, R.M. Wallace, K.A. Cychosz, M. Thommes, D. Su, E.A. Stach, R.S. Ruoff, Carbon-based supercapacitors produced by activation of graphene, Science 332 (2011) 1537–1541.
[22] C. Portet, G. Yushin, Y. Gogotsi, Electrochemical performance of carbon onions, nanodiamonds, carbon black and multiwalled nanotubes in electrical double layer capacitors, Carbon 45 (2007) 2511–2518.
[23] D. Pech, M. Brunet, H. Durou, P. Huang, V. Mochalin, Y. Gogotsi, P.L. Taberna, P. Simon, Ultrahigh-power micrometre-sized supercapacitors based on onion-like carbon, Nat. Nanotechnol. 5 (2010) 651–654.
[24] G. Moussa, C.M. Ghimbeu, P.L. Taberna, P. Simon, C. Vix-Guterl, Relationship between the carbon nano-onions (CNOs) surface chemistry/defects and their capacitance in aqueous and organic electrolytes, Carbon 105 (2016) 628–637.
[25] E. Frackowiak, K. Jurewicz, S. Delpeux, F. Beguin, Electrochemical application of carbon nanotubes, Nato. Sci. Ser. Ii-Math. 91 (2003) 305–318.
[26] C. Vix-Guterl, E. Frackowiak, K. Jurewicz, M. Friebe, J. Parmentier, F. Beguin, Electrochemical energy storage in ordered porous carbon materials, Carbon 43 (2005) 1293–1302.
[27] A.B. Fuertes, G. Lota, T.A. Centeno, E. Frackowiak, Templated mesoporous carbons for supercapacitor application, Electrochim. Acta 50 (2005) 2799–2805.
[28] F. Béguin, E. Frąckowiak, Carbons for Electrochemical Energy Storage and Conversion Systems, CRC Press, New York, 2009.
[29] V. Presser, M. Heon, Y. Gogotsi, Carbide-derived carbons - from porous networks to nanotubes and graphene, Adv. Funct. Mater. 21 (2011) 810–833.
[30] Y. Soneda, Carbons for Supercapacitors, 2013, pp. 211–222.
[31] D.S. Su, G. Centi, A perspective on carbon materials for future energy application, J. Energy Chem. 22 (2013) 151–173.
[32] K.L. Van Aken, C.R. Pérez, Y. Oh, M. Beidaghi, Y. Joo Jeong, M.F. Islam, Y. Gogotsi, High rate capacitive performance of single-walled carbon nanotube aerogels, Nanomater. Energy 15 (2015) 662–669.
[33] B. Dyatkin, O. Gogotsi, B. Malinovskiy, Y. Zozulya, P. Simon, Y. Gogotsi, High capacitance of coarse-grained carbide derived carbon electrodes, J. Power Sources 306 (2016) 32–41.
[34] B. Anasori, M.R. Lukatskaya, Y. Gogotsi, 2D metal carbides and nitrides (MXenes) for energy storage, Nat. Rev. Mater. 2 (2017).
[35] E. Raymundo-Pinero, K. Kierzek, J. Machnikowski, F. Beguin, Relationship between the nanoporous texture of activated carbons and their capacitance properties in different electrolytes, Carbon 44 (2006) 2498–2507.
[36] D.Y. Qu, Studies of the activated carbons used in double-layer supercapacitors, J. Power Sources 109 (2002) 403–411.
[37] P.J. Hall, M. Mirzaeian, S.I. Fletcher, F.B. Sillars, A.J.R. Rennie, G.O. Shitta-Bey, G. Wilson, A. Cruden, R. Carter, Energy storage in electrochemical capacitors: designing functional materials to improve performance, Energy Environ. Sci. 3 (2010) 1238–1251.
[38] P. Gonzalez-Garcia, Activated carbon from lignocellulosics precursors: a review of the synthesis methods, characterization techniques and applications, Renew. Sustain. Energy Rev. 82 (2018) 1393–1414.
[39] A.J. Romero-Anaya, M. Ouzzine, M.A. Lillo-Rodenas, A. Linares-Solano,

Spherical carbons: synthesis, characterization and activation processes, Carbon 68 (2014) 296–307.
[40] Y. Liu, Y. Guo, Y. Zhu, D. An, W. Gao, Z. Wang, Y. Ma, Z. Wang, A sustainable route for the preparation of activated carbon and silica from rice husk ash, J. Hazard Mater. 186 (2011) 1314–1319.
[41] J. Laine, S. Yunes, Effect of the preparation method on the pore-size distribution of activated carbon from coconut shell, Carbon 30 (1992) 601–604.
[42] C. Decaux, C.M. Ghimbeu, M. Dahbi, M. Anouti, D. Lemordant, F. Beguin, C. Vix-Guterl, E. Raymundo-Pinero, Influence of electrolyte ion-solvent interactions on the performances of supercapacitors porous carbon electrodes, J. Power Sources 263 (2014) 130–140.
[43] J.A. Macia-Agullo, B.C. Moore, D. Cazorla-Amoros, A. Linares-Solano, Activation of coal tar pitch carbon fibres: physical activation vs. chemical activation, Carbon 42 (2004) 1367–1370.
[44] S.H. Yoon, S. Lim, Y. Song, Y. Ota, W.M. Qiao, A. Tanaka, I. Mochida, KOH activation of carbon nanofibers, Carbon 42 (2004) 1723–1729.
[45] C. Merlet, C. Pean, B. Rotenberg, P.A. Madden, B. Daffos, P.L. Taberna, P. Simon, M. Salanne, Highly confined ions store charge more efficiently in supercapacitors, Nat. Commun. 4 (2013) 2701.
[46] A. Garcia-Gomez, V. Barranco, G. Moreno-Fernandez, J. Ibanez, T.A. Centeno, J.M. Rojo, Correlation between capacitance and porosity in microporous carbon monoliths, J. Phys. Chem. C 118 (2014) 5134–5141.
[47] F. Stoeckli, T.A. Centeno, Pore size distribution and capacitance in microporous carbons, Phys. Chem. Chem. Phys. 14 (2012) 11589–11591.
[48] O. Barbieri, M. Hahn, A. Herzog, R. Kotz, Capacitance limits of high surface area activated carbons for double layer capacitors, Carbon 43 (2005) 1303–1310.
[49] L. Zhang, F. Zhang, X. Yang, G. Long, Y. Wu, T. Zhang, K. Leng, Y. Huang, Y. Ma, A. Yu, Y. Chen, Porous 3D graphene-based bulk materials with exceptional high surface area and excellent conductivity for supercapacitors, Sci. Rep. 3 (2013) 1408.
[50] A.G. Pandolfo, A.F. Hollenkamp, Carbon properties and their role in supercapacitors, J. Power Sources 157 (2006) 11–27.
[51] J. Chmiola, G. Yushin, R. Dash, Y. Gogotsi, Effect of pore size and surface area of carbide derived carbons on specific capacitance, J. Power Sources 158 (2006) 765–772.
[52] M. Inagaki, M. Toyoda, Y. Soneda, S. Tsujimura, T. Morishita, Templated mesoporous carbons: synthesis and applications, Carbon 107 (2016) 448–473.
[53] G. Hasegawa, K. Kanamori, T. Kiyomura, H. Kurata, T. Abe, K. Nakanishi, Hierarchically porous carbon monoliths comprising ordered mesoporous nanorod assemblies for high-voltage aqueous supercapacitors, Chem. Mater. 28 (2016) 3944–3950.
[54] J. Lee, J. Kim, T. Hyeon, Recent progress in the synthesis of porous carbon materials, Adv. Mater. 18 (2006) 2073–2094.
[55] W.R. Li, D.H. Chen, Z. Li, Y.F. Shi, Y. Wan, G. Wang, Z.Y. Jiang, D.Y. Zhao, Nitrogen-containing carbon spheres with very large uniform mesopores: the superior electrode materials for EDLC in organic electrolyte, Carbon 45 (2007) 1757–1763.
[56] C. Liang, Z. Li, S. Dai, Mesoporous carbon materials: synthesis and modification, Angew Chem. Int. Ed. Engl. 47 (2008) 3696–3717.
[57] A. Huczko, Template-based synthesis of nanomaterials, Appl. Phys. Mater. 70 (2000) 365–376.
[58] W. Libbrecht, A. Verberckmoes, J.W. Thybaut, P. Van der Voort, J. De Clercq, Soft templated mesoporous carbons: tuning the porosity for the adsorption of large organic pollutants, Carbon 116 (2017) 528–546.
[59] J. Liu, T.Y. Yang, D.W. Wang, G.Q.M. Lu, D.Y. Zhao, S.Z. Qiao, A facile soft-template synthesis of mesoporous polymeric and carbonaceous nanospheres, Nat. Commun. 4 (2013).
[60] Q. Li, R.R. Jiang, Y.Q. Dou, Z.X. Wu, T. Huang, D. Feng, J.P. Yang, A.S. Yu, D.Y. Zhao, Synthesis of mesoporous carbon spheres with a hierarchical pore structure for the electrochemical double-layer capacitor, Carbon 49 (2011) 1248–1257.
[61] T. Kyotani, Control of pore structure in carbon, Carbon 38 (2000) 269–286.
[62] S. Zhu, P.L. Taberna, N.Q. Zhao, P. Simon, Salt-template synthesis of mesoporous carbon monolith for ionogel-based supercapacitors, Electrochem. Commun. 96 (2018) 6–10.
[63] T. Kyotani, J. Chmiola, Y. Gogotsi, Carbide-derived carbons and templated carbons, Adv. Mat. Tech. Ser. (2010) 77–113.
[64] E. Masika, R. Mokaya, High surface area metal salt templated carbon aerogels via a simple subcritical drying route: preparation and CO2 uptake properties, RSC Adv. 3 (2013) 17677–17681.
[65] N. Fechler, T.P. Fellinger, M. Antonietti, Salt templating": a simple and sustainable pathway toward highly porous functional carbons from ionic liquids, Adv. Mater. 25 (2013) 75–79.
[66] D. Qiu, T. Cao, J. Zhang, S.-W. Zhang, D. Zheng, H. Wu, W. Lv, F. Kang, Q.-H. Yang, Precise carbon structure control by salt template for high performance sodium-ion storage, J. Energy Chem. 31 (2019) 101–106.
[67] C. Nita, M. Bensafia, C. Vaulot, L. Delmotte, C.M. Ghimbeu, Insights on the synthesis mechanism of green phenolic resin derived porous carbons via a salt-soft templating approach, Carbon 109 (2016) 227–238.
[68] C.M. Ghimbeu, L. Vidal, L. Delmotte, J.M. Le Meins, C. Vix-Guterl, Catalyst-free soft-template synthesis of ordered mesoporous carbon tailored using phloroglucinol/glyoxylic acid environmentally friendly precursors, Green Chem. 16 (2014) 3079–3088.
[69] D.W. Wang, F. Li, M. Liu, G.Q. Lu, H.M. Cheng, 3D aperiodic hierarchical porous graphitic carbon material for high-rate electrochemical capacitive energy storage, Angew Chem. Int. Ed. Engl. 47 (2008) 373–376.
[70] T.Q. Lin, I.W. Chen, F.X. Liu, C.Y. Yang, H. Bi, F.F. Xu, F.Q. Huang, Nitrogen-doped mesoporous carbon of extraordinary capacitance for electrochemical energy storage, Science 350 (2015) 1508–1513.
[71] S. Alvarez, M.C. Blanco-Lopez, A.J. Miranda-Ordieres, A.B. Fuertes, T.A. Centeno, Electrochemical capacitor performance of mesoporous carbons obtained by templating technique, Carbon 43 (2005) 866–870.
[72] J. Jagiello, J.P. Olivier, 2D-NLDFT adsorption models for carbon slit-shaped pores with surface energetical heterogeneity and geometrical corrugation, Carbon 55 (2013) 70–80.
[73] C. Nita, J. Fullenwarth, L. Monconduit, J.M. Le Meins, P. Fioux, J. Parmentier, C.M. Ghimbeu, Eco-friendly synthesis of SiO2 nanoparticles confined in hard carbon: a promising material with unexpected mechanism for Li-ion batteries, Carbon 143 (2019) 598–609.
[74] C. Largeot, C. Portet, J. Chmiola, P.L. Taberna, Y. Gogotsi, P. Simon, Relation between the ion size and pore size for an electric double-layer capacitor, J. Am. Chem. Soc. 130 (2008) 2730–2731.
[75] Q. Abbas, D. Pajak, E. Frackowiak, F. Beguin, Effect of binder on the performance of carbon/carbon symmetric capacitors in salt aqueous electrolyte, Electrochim. Acta 140 (2014) 132–138.
[76] N. Shimodaira, A. Masui, Raman spectroscopic investigations of activated carbon materials, J. Appl. Phys. 92 (2002) 902–909.
[77] J. Menzel, E. Frackowiak, K. Fic, Electrochemical capacitor with water-based electrolyte operating at wide temperature range, J. Power Sources 414 (2019) 183–191.
[78] C. Vix-Guterl, M. Couzi, J. Dentzer, M. Trinquecoste, P. Delhaes, Surface characterizations of carbon multiwall nanotubes: comparison between surface active sites and Raman Spectroscopy, J. Phys. Chem. B 108 (2004) 19361–19367.
[79] M.S. Dresselhaus, A. Jorio, M. Hofmann, G. Dresselhaus, R. Saito, Perspectives on carbon nanotubes and graphene Raman spectroscopy, Nano Lett. 10 (2010) 751–758.
[80] L. Demarconnay, E. Raymundo-Pinero, F. Beguin, A symmetric carbon/carbon supercapacitor operating at 1.6 V by using a neutral aqueous solution, Electrochem. Commun. 12 (2010) 1275–1278.
[81] J.H. Chae, G.Z. Chen, 1.9 V aqueous carbon-carbon supercapacitors with unequal electrode capacitances, Electrochim. Acta 86 (2012) 248–254.
[82] K. Fic, G. Lota, M. Meller, E. Frackowiak, Novel insight into neutral medium as electrolyte for high-voltage supercapacitors, Energy Environ. Sci. 5 (2012) 5842–5850.
[83] Q. Gao, Optimizing carbon/carbon supercapacitors in aqueous and organic electrolytes, Chemistry, Université d'Orléans, CRMD - Centre de Recherche sur la Matière Divisée (2013) 1–155.
[84] H.C. Chien, T.H. Wu, M. Rajkumar, C.C. Hu, Effects of buffer agents on hydrogen adsorption and desorption at/within activated carbon for the negative electrode of aqueous asymmetric supercapacitors, Electrochim. Acta 205 (2016) 1–7.
[85] A. Slesinski, C. Matei-Ghimbeu, K. Fic, F. Beguin, E. Frackowiak, Self-buffered pH at carbon surfaces in aqueous supercapacitors, Carbon 129 (2018) 758–765.
[86] K. Jurewicz, E. Frackowiak, F. Beguin, Towards the mechanism of electrochemical hydrogen storage in nanostructured carbon materials, Appl. Phys. Mater. 78 (2004) 981–987.
[87] F. Béguin, M. Friebe, K. Jurewicz, C. Vix-Guterl, J. Dentzer, E. Frackowiak, State of hydrogen electrochemically stored using nanoporous carbons as negative electrode materials in an aqueous medium, Carbon 44 (2006) 2392–2398.
[88] F. Beguin, K. Kierzek, M. Friebe, A. Jankowska, J. Machnikowski, K. Jurewicz, E. Frackowiak, Effect of various porous nanotextures on the reversible electrochemical sorption of hydrogen in activated carbons, Electrochim. Acta 51 (2006) 2161–2167.
[89] K. Fic, M. He, E.J. Berg, P. Novák, E. Frackowiak, Comparative operando study of degradation mechanisms in carbon-based electrochemical capacitors with Li2SO4 and LiNO3 electrolytes, Carbon 120 (2017) 281–293.
[90] M. He, K. Fic, E. Frąckowiak, P. Novák, E.J. Berg, Towards more durable electrochemical capacitors by elucidating the ageing mechanisms under different testing procedures, Chemelectrochem 6 (2019) 566–573.
[91] P. Ratajczak, K. Jurewicz, F. Beguin, Factors contributing to ageing of high voltage carbon/carbon supercapacitors in salt aqueous electrolyte, J. Appl. Electrochem. 44 (2014) 475–480.
[92] M. Meller, K. Fic, Effect of benzoquinone additives on the performance of symmetric carbon/carbon capacitors - electrochemical impedance study, J. Energy Stor. 18 (2018) 340–348.